PERGAMON

International Journal of Heat and Mass Transfer 41 (1998) 4229–4249

International Journal of HEAT and MASS TRANSFER

Modeling forced liquid convection in rectangular microchannels with electrokinetic effects

Chun Yang[a], Dongqing Li[a,*], Jacob H. Masliyah[b]

[a] *Department of Mechanical Engineering, University of Alberta, Edmonton, Alberta, T6G 2G8, Canada*
[b] *Department of Chemical Engineering, University of Alberta, Edmonton, Alberta, T6G 2G6, Canada*

Received 9 September 1997; in final form 18 March 1998

Abstract

The effects of the electric double layer near the solid–liquid interface and the flow induced electrokinetic field on the pressure-driven flow and heat transfer through a rectangular microchannel are analyzed in this work. The electric double layer field in the cross-section of rectangular microchannels is determined by solving a non-linear, two-dimensional Poisson–Boltzmann equation. A body force caused by the electric double field and the flow-induced electrokinetic field is considered in the equation of motion. For steady-state, fully-developed laminar flows, both the velocity and the temperature fields in a rectangular microchannel are determined for various conditions. The flow and heat transfer characteristics with/without consideration of the electrokinetic effects are evaluated. The results clearly show that, for aqueous solutions of low ionic concentrations and a solid surface of high zeta potential, the liquid flow and heat transfer in rectangular microchannels are significantly influenced by the presence of the electric double layer field and the induced electrokinetic flow.

Nomenclature

A_c cross-section area of the channel [m^2]
C_f friction coefficient
C_{pf} specific heat capacity of liquid [$J\ kg^{-1}\ K^{-1}$]
D_h channel hydraulic diameter [m]
e elementary charge [C]
Ec Eckert number
EDL electrical double layer
E_x streaming potential [$V\ m^{-1}$]
f friction factor
G_1, G_2 non-dimensional parameters
h_x local heat transfer coefficient [$W\ m^{-2}\ K^{-1}$]
H channel height [m]
I_c, I_s conduction and streaming current, respectively [A]
k_b Boltzmann constant [$J\ mol^{-1}\ K^{-1}$]
K non-dimensional electrokinetic diameter
L channel length [m]
n_+, n_- local concentration of positive and negative ions, respectively [m^{-3}]
n_0 bulk concentration of ions [m^{-3}]
Nu Nusselt number
P hydraulic pressure in x-direction [Pa]
Pe Peclet number
Pr Prandtl number
P_S channel perimeter [m]
q'' heat flux [$W\ m^{-2}$]
Q_v, Q_{0v} volume flow rate with and without EDL effects, respectively [$m^3\ s^{-1}$]
Re_0 reference Reynolds number
T temperature [K]
u fluid velocity component in x flow direction [$m\ s^{-1}$]
u_{ave}, u_{0ave} average fluid velocity with and without EDL effects, respectively [$m\ s^{-1}$]
U reference velocity [$m\ s^{-1}$]
v, w fluid velocity component in y and z direction, respectively [$m\ s^{-1}$]
W half channel width [m]
X, $\bar{X}$ non-dimensional x-coordinate
Y, Z non-dimensional y-coordinate and z-coordinate, respectively
z_+, z_- valence of the positive and negative ions, respectively.

* Corresponding author. Tel.: 001 403 492 9734; fax: 001 403 492 2200; e-mail: dongqing.li@ualberta.ca

0017–9310/98 $19.00
PII: S0017–9310(98)00125–2

Greek symbols

α_f thermal diffusivity of the fluid [$m^2 s^{-1}$]
ε_r dielectric constant of the fluid
ε_0 permittivity of vacuum [$C V^{-1} m^{-1}$]
θ temperature of the fluid [K]
$\bar{\theta}$ non-dimensional temperature of the fluid
κ Debye–Huckel parameter [m^{-1}]
κ_f thermal conductivity of the fluid [$W m^{-1} K^{-1}$]
λ_b, λ_s bulk and surface electric conductivity of the fluid, respectively [$1 \Omega^{-1} m^{-1}$]
μ_a apparent viscosity of the fluid [$kg m^{-1} s^{-1}$]
μ_f dynamic viscosity of the fluid [$kg m^{-1} s^{-1}$]
ζ zeta potential [V]
ρ_e net electric charge density [$C m^{-3}$]
ρ_f density of the fluid [$kg m^{-3}$]
ψ local electrostatic potential in the EDL [V]
Ψ non-dimensional electrical potential.

Superscript

$\bar{}$ non-dimensional parameters.

1. Introduction

Understanding of microscale transport phenomena is important to the design and process control of various Micro-Electric-Mechanical Systems (MEMS) and many modern instruments used in chemical analysis and biomedical diagnostics. The microchannel heat exchanger or microchannel heat sink is such an example [1]. Microchannel heat sinks have a great potential for cooling high power VLSI circuitry [2] and high power laser diode arrays [3]. However, many experimental observations [4] have shown that heat transfer and flow phenomena in microscale are quite different from those in macroscale. It is, therefore, necessary to study the fundamental characteristics of these phenomena in order to develop the related high technology products.

Since the pioneering work of Tuckerman and Pease [2], a significant amount of experimental information has been generated in the areas of forced flow and convection heat transfer in microchannels [4, 5]. Anomalous behaviors of microchannel flow and heat transfer were observed by some investigators in their experiments. Pfahler et al. [6, 7] conducted an experimental investigation of fluid flow in microchannels. They found that in relatively large flow channels, the experimental observations were in a rough agreement with the predictions from classical theories. However, deviations from the classical Poiseuille flow were observed in the small channels (hydraulic diameter less than 40 μm). This may imply that certain phenomena become important at smaller channels or that the conventional form of the Navier–Stokes equation is not adequate for modeling microchannel flow. Moreover, their results indicate that polar fluids (isopropanol) and non-polar fluids (silicon oil) behave differently, and thus polar nature of the fluid may play a role in the microchannel flow. Similarly, Urbanek et al. [8] measured liquid (1- and 2-propanol, 1- and 3-pentanol, and water) flow through 5, 12 and 25 μm hydraulic diameter microchannels with liquid temperature varying from 0–85°C. The Poiseuille number (i.e., friction coefficient) dependence on fluid temperature and the channel size was reported (according to the conventional theories, the Poiseuille number should be independent of fluid properties and only a function of the cross-section of the channel). Also the ratio of the measured friction coefficient to the predicted friction coefficient was found to change from 1.01–1.30 depending on the working fluid and the temperature. Muhammad and Gui [9] performed experimental measurement of water flow and heat transfer in silicon wafer microchannels with different ratios of height to width. Their experiments showed that the friction coefficient is slightly higher than that predicted by classical theories. Again the significantly high heat transfer coefficient in microchannels (compared with that in macrochannels) was obtained. More recently, Peng and Wang [10] and Peng and Peterson [11] systematically examined the forced flow and heat transfer characteristics of water and binary mixtures flowing through rectangular microchannels. It was observed that the laminar flow transition occurred at Reynolds number between 200 and 700, and the critical transition Reynolds number diminished with the decrease in the size of the microchannels. Furthermore, the strong effects of the hydraulic diameter and the aspect ratio on the flow and heat transfer in microchannels were found. Overall, these investigations provided substantial experimental data and considerable evidence that the flow and heat transfer in microchannels are strongly dependent upon the type and properties of the working fluid as well as geometric parameters of microchannels [12], and therefore may be quite different from what typically occur in macrochannels.

On the theoretical side, Eringen [13, 14] extended continuum fluid theory to describe microfluid behavior. He proposed a microcontinuum theory to describe the translation, rotation, and deformation of individual fluid elements. He stated that the fluid flow in microchannels will deviate from the prediction of the classical N–S equation. Later Jacobi [15] employed this microcontinuum theory to a fully developed, laminar convection in a circular duct with constant heat flux. The 'distorted' velocity and temperature profiles (compared with the conventional profiles) were reported. Jacobi also showed that Nusselt number is reduced by as much as 7% for polar fluids from the theoretical value of 4.36. In addition, slip flow theory, based on the rarefied dynamic model, has also been introduced to model microscale flows [16, 17]. Nevertheless, as pointed out by Duncan and Peterson [4] in their excellent review of microscale heat transfer, little fundamental work on the microchannel flow and heat transfer has been done since the early work by Eringen.

The objective of this paper is to evaluate the influence of interfacial electrokinetic phenomena on the flow and heat transfer in rectangular microchannels, in an attempt to provide insight into mechanisms of microchannel flow and heat transfer. In this study we believe that the electrical double layer near the liquid–channel wall interface and the electrokinetic flow may be responsible for these unusual behaviors of the microchannel flow and heat transfer. It is known that most solid surfaces carry electrostatic charges, i.e. an electrical surface potential. If the liquid contains a very small number of ions (for instance, due to impurities), the electrostatic charges on the non-conducting solid surface will attract the counterions in the liquid. The rearrangement of the charges on the solid surface and the balancing charges in the liquid is called the electrical double layer (EDL) [18]. Because of the electrostatic interaction, the counterion concentration near the solid surface is higher than that in the bulk liquid far away from the solid surface. Immediately next to the solid surface, there is a layer of counterions which are strongly attracted to the solid surface and are immobile. This layer is called the compact layer, normally about several Angstroms thick. From the compact layer to the uniform bulk liquid, the counterion concentration gradually reduces to that of bulk liquid. Ions in this region are affected less by the electrostatic interaction and are mobile. This layer is called the diffuse layer of the EDL. The thickness of the diffuse layer is dependent on the bulk ionic concentration and electrical properties of the liquid, usually ranging from several nanometers for high ionic concentration solutions up to the order of microns for distilled water. Generally, for macrochannel flow the EDL effects can be safely neglected as the thickness of the EDL is very small compared with the characteristic size of channels. However, for microchannel flow the thickness of the EDL is often comparable with the characteristic size of flow channels. Thus the EDL effects originated from the electrostatic interaction between ions in liquid and the charged solid (flow channel) surface may play an important role in microchannel flow and heat transfer.

When a liquid is forced through a microchannel under an applied hydrostatic pressure, the counterions in the diffuse layer (mobile part) of the EDL are moving towards the downstream end. The movement of counterions or electrical charges, however, generates an electric field with an electrokinetic potential called the streaming potential [18]. This induced streaming potential is a steady-state potential difference which builds up along a microchannel. The presence of the EDL field and the streaming potential will exert electric forces on the ions in the diffuse double layer, and hence have a profound influence on the motion of ions. It is obvious that when ions move in a liquid, they will pull the liquid molecules to move with them. Therefore, the liquid flow and hence the heat transfer are affected by the presence of the EDL field and the streaming potential. Such phenomenon are usually referred to as electrokinetic effects [18].

The theory of the electrokinetic effects on microchannel flow characteristics has been well established [19]. Burgreen and Nakache [20] studied the effect of the surface potential on liquid transport through ultrafine capillary slits with the Debye–Huckel linear approximation to the electrical potential distribution under an imposed electrical field. Rice and Whitehead [21] conducted a research on the same problem in narrow cylindrical capillaries. Levine et al. [22] extended Rice and Whitehead's model to a higher surface potential by developing an approximate solution of the Poisson–Boltzmann (P–B) equation. Recently, Mala et al. [23] presented a paper on a microchannel flow and heat transfer between two parallel plates with electrokinetic effects. In addition to the above mentioned theoretical studies, the experimental evidence of the electrokinetic effects on the liquid flow in microchannels were also provided in the literature [19]. More recently, Mala et al. [24] reported experimental studies of flow of distilled water and aqueous solutions through silicon and glass microchannels between two parallel plates. Microchannels with a height ranging from 10–280 μm were used in their measurements. Their results amply demonstrated that the liquid flow in such a microchannel was strongly influenced by the electrokinetic effects. For example, depending on the channel height and the electrical properties of the channel surface, the measured flow rate of the distilled water can be 80% lower than that predicted from the classical Poiseuille flow equation.

Generally, most of these cited studies of electrokinetic effects on liquid flow dealt with one-dimensional EDL field, which holds only for simple geometric channels, such as circular cylinders and slit-shaped channels. No study has been reported to consider the electrokinetic effects on the forced flow in rectangular microchannels. However, in practice, the cross-section of microchannels made by modern micromachining technology is close to a rectangular shape [25]. In such a situation, a two-dimensional P–B equation is required to describe the electrical potential distribution in the rectangular channel; and the corner of the channel may have particular contribution to the EDL field, subsequently to the fluid flow and heat transfer.

To evaluate the electrokinetic effects on the microchannel liquid flow and heat transfer, our focus in this paper is restricted to a steady-state, fully-developed, laminar liquid flow and convection in rectangular microchannels. First, a non-linear, two-dimensional Poisson–Boltzmann (P–B) equation is solved numerically. Then an additional body force originating from the electrical double layer (EDL) and the electrokinetic fields is introduced to the conventional Navier–Stokes (N–S) equation. Following that a procedure is developed to obtain

an exact solution to the modified N–S equation. Finally, the general energy equation for rectangular microchannels is constructed and the calculations for the energy equation are carried out. The flow and heat transfer characteristics with/without consideration of the EDL effects are compared and discussed.

2. Electrical double layer field in a rectangular microchannel

In order to consider the EDL and the electrokinetic effects on the fluid flow in rectangular microchannels, we must evaluate the distributions of electrical potentials and net charge density in a rectangular microchannel. Consider a rectangular microchannel of width $2W$, height H, and length L as illustrated in Fig. 1(a). According to the theory of electrostatics, the relationship between the electrical potential ψ and the net charge density per unit volume ρ_e at any point in the solution is described by the two-dimensional Poisson equation

$$\frac{\partial^2\psi}{\partial y^2}+\frac{\partial^2\psi}{\partial z^2}=-\frac{\rho_e}{\varepsilon_r\varepsilon_0} \tag{1}$$

where ε_r is the dielectric constant of the solution and ε_0 is the permittivity of vacuum.

Assuming the Boltzmann distribution equation is applicable, the number concentration of the type-i ion in a symmetric electrolyte solution is of the form

$$n_i=n_{i0}\exp\left(-\frac{z_i e\psi}{k_b T}\right) \tag{2}$$

where n_{i0} and z_i are the bulk concentration and the valence of type-i ions, respectively, e is the elementary charge, k_b is the Boltzmann constant, and T is the absolute temperature. Strictly speaking, the Boltzmann distribution is applicable only when the system is in equilibrium state. If there exists a liquid flow, the ionic concentration distribution may be distorted by the presence of the flow and hence should be described by the general Nernst–Planck [26] (i.e., the particle mass transfer) equation. In such a case, the problem may become more difficult to deal with since the Poisson equation, the Nernst–Planck equation, and the equation of motion are coupled. However, in the literature many previous studies [19–23] simply assumed that the Boltzmann distribution is applicable without giving any proof. As such, the validity of Boltzmann distribution applicable to the microchannel flow has been examined in this study. It was found that only for a microchannel flow with a very small Peclet number or in a fully-developed hydrodynamic state, the Boltzmann distribution can be safely applied. The detailed proof is given in Appendix A.

The net volume charge density ρ_e is proportional to the concentration difference between symmetric cations and anions, via

$$\rho_e=ze(n_+-n_-)=-2zen_0\sinh\left(\frac{ze\psi}{k_b T}\right). \tag{3}$$

Substituting equation (3) into the Poisson equation leads to the well-known Poisson–Boltzmann equation.

$$\frac{\partial^2\psi}{\partial y^2}+\frac{\partial^2\psi}{\partial z^2}=\frac{2zen_0}{\varepsilon_r\varepsilon_0}\sinh\left(\frac{ze\psi}{k_b T}\right). \tag{4}$$

By defining the Debye–Huckel parameter $\kappa=(2z^2e^2n_0/\varepsilon_r\varepsilon_0k_bT)^{1/2}$ ($1/\kappa$ is normally referred to as the EDL thickness) and the hydraulic diameter of the rectangular microchannel $D_h=4HW/(H+2W)$ and introducing the dimensionless groups: $Y=y/D_h$, $Z=z/D_h$, $K=\kappa D_h$, and $\Psi=ze\psi/k_bT$, the above equation can be non-dimensionalized as

$$\frac{\partial^2\Psi}{\partial Y^2}+\frac{\partial^2\Psi}{\partial Z^2}=K^2\sinh\Psi \tag{5}$$

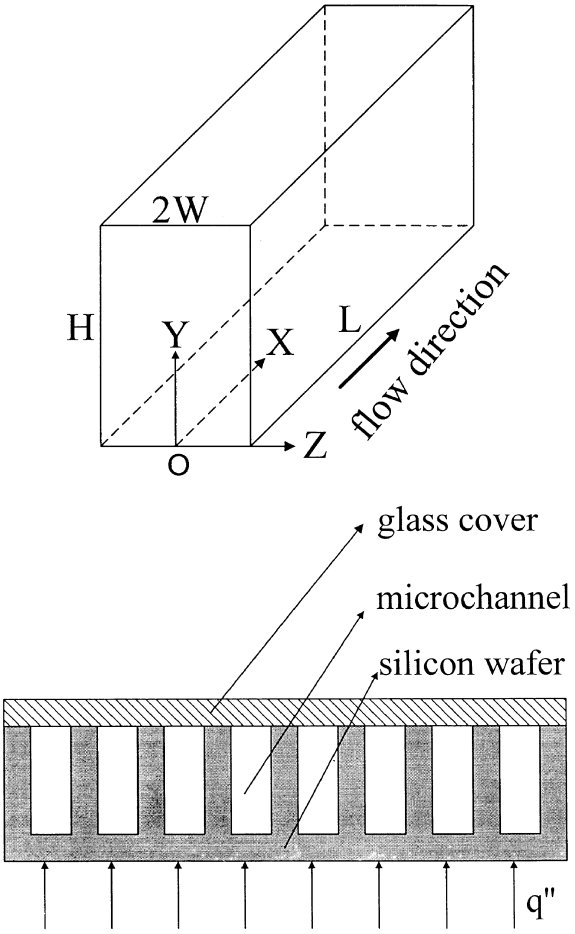

Fig. 1. (a) A rectangular microchannel (width $2W$, height H, length L). (b) Schematic of the microchannel cooling system.

here Y and Z are non-dimensional coordinates shown in Fig. 1, K is the non-dimensional electrokinetic diameter defined as the ratio of the hydraulic diameter to the electrical double layer thickness, and Ψ is the non-dimensional electrical potential representing the ratio of the electrical energy $ze\psi$ to the thermal energy k_bT.

Due to the symmetry of a rectangular channel, equation (5) is subjected to the following boundary conditions in a half of the rectangular cross-section:

$$Y=0 \quad \Psi=\bar{\zeta} \quad Y=\frac{H}{D_h} \quad \Psi=\bar{\zeta} \tag{6a}$$

$$Z=0 \quad \frac{\partial\Psi}{\partial Z}=0 \quad Z=\frac{W}{D_h} \quad \Psi=\bar{\zeta} \tag{6b}$$

where $\bar{\zeta}$, defined by $\bar{\zeta}=ze\zeta/k_bT$, is a non-dimensional zeta potential of the channel walls (here ζ is the zeta potential of the channel wall). The zeta potential is a measurable electrical potential at the shear plane, i.e. the boundary between the compact layer and the diffuse layer, as defined in the EDL theory [18].

In order to solve this non-linear, elliptic, differential equation, a numerical finite-difference scheme [27] is introduced to derive this differential equation into discrete, algebraic equations. The non-linear source term in equation (5) is linearized as

$$\sinh\Psi_{n+1}=\sinh\Psi_n+(\Psi_{n+1}-\Psi_n)\cosh\Psi_n \tag{7}$$

where the subscript $(n+1)$ and n represent the $(n+1)$th and the nth iterative value, respectively. The derived discrete, algebraic equations are solved by using the Gauss–Seidel iterative procedure. The solution of the linearized P–B equation with the same boundary conditions is chosen as the first guess value for the iterative calculation. The under-relaxation technique is employed to make this iterative process converge quickly. The criterion of numerical convergence is chosen as 10^{-4}, which is the relative desired accuracy (given as $|\Psi_{n+1}-\Psi_n|/\Psi_n\leqslant 10^{-4}$) for the calculated non-dimensional potential values at each grid point on two successive iterations.

After the electrical potential inside the rectangular microchannel is computed, the local net charge density can be obtained from equation (3) as

$$\rho_e(Y,Z)=-2zen_0\sinh\Psi(Y,Z) \tag{8}$$

This local net charge density is required to determine electrostatic force caused by the presence of the EDL field. Such an electrostatic force is considered as an additional body force existing in microchannel flow to modify the conventional Poiseuille flow equation, which will be discussed in the next section.

3. Flow field in a rectangular microchannel

Consider the case of a two-dimensional, forced, laminar flow through a rectangular microchannel as illustrated in Fig. 1(a). The equation of motion for an incompressible liquid is given by

$$\rho_f\frac{\partial\mathbf{V}}{\partial t}+\rho_f(\mathbf{V}\cdot\nabla)\mathbf{V}=-\nabla P+\mathbf{F}+\mu_f\nabla^2\mathbf{V}. \tag{9}$$

In this equation, ρ_f and μ_f are the density and viscosity of the liquid, respectively. For a steady-state, fully developed flow, the components of velocity $\mathbf{V}$ satisfy $u=u(y,z)$ and $v=w=0$ in terms of Cartesian coordinates. Thus, both the time term $\partial\mathbf{V}/\partial t$ and the inertia term $(\mathbf{V}\cdot\nabla)\mathbf{V}$ vanish. Also, the hydraulic pressure P is a function of x only and the pressure gradient $\mathrm{d}P/\mathrm{d}x$ is constant. If the gravity effect is negligible, the body force $\mathbf{F}$ is caused only by the action of an induced electrical field E_x (see the explanation in the electrokinetic potential section) on the net charge density $\rho_e(Y,Z)$ [determined from equation (8)] in the electric double layer region, i.e. $F_x=E_x\rho_e$. With these considerations, equation (9) is reduced to

$$\frac{\partial^2u}{\partial y^2}+\frac{\partial^2u}{\partial z^2}=\frac{1}{\mu_f}\frac{\mathrm{d}P}{\mathrm{d}x}-\frac{1}{\mu_f}E_x\rho_e(y,z). \tag{10}$$

Defining the reference Reynolds number $Re_0=\rho_fD_hU/\mu_f$ and non-dimensionalizing equation (10) via the following dimensionless parameters

$$\bar{u}=\frac{u}{U} \quad \bar{P}=\frac{P-P_0}{\rho_fU^2} \quad \bar{X}=\frac{x}{D_h\,Re_0} \tag{11a}$$

$$\frac{\mathrm{d}\bar{P}}{\mathrm{d}\bar{X}}=\frac{D_h\,Re_0}{\rho_fU^2}\frac{\mathrm{d}P}{\mathrm{d}x} \quad \bar{E}_x=\frac{E_xD_h\,Re_0}{\zeta_0} \tag{11b}$$

where U is a reference velocity, P_0 is a reference pressure, and ζ_0 is a reference electrical potential, one can obtain the non-dimensionalized equation of motion

$$\frac{\partial^2\bar{u}}{\partial Y^2}+\frac{\partial^2\bar{u}}{\partial Z^2}=\frac{\mathrm{d}\bar{P}}{\mathrm{d}\bar{X}}-\frac{\psi_e}{\rho_fU^2}\bar{E}_x\rho_e(Y,Z). \tag{12}$$

Substituting $\rho_e(Y,Z)$ by equation (8) and defining a new dimensionless number $\bar{G}_1=2zen_0\zeta_0/\rho_fU^2$, the equation of motion may, therefore, be written as

$$\frac{\partial^2\bar{u}}{\partial Y^2}+\frac{\partial^2\bar{u}}{\partial Z^2}=\frac{\mathrm{d}\bar{P}}{\mathrm{d}\bar{X}}+\bar{G}_1\bar{E}_x\sinh\Psi(Y,Z). \tag{13}$$

The symmetric and no-slip boundary conditions that apply for the velocity $\bar{u}$ are

$$Y=0 \quad \bar{u}=0 \quad Y=\frac{H}{D_h} \quad \bar{u}=0 \tag{14a}$$

$$Z=0 \quad \frac{\partial\bar{u}}{\partial Z}=0 \quad Z=\frac{W}{D_h} \quad \bar{u}=0. \tag{14b}$$

It is worth mentioning here that the present model is within the frame of the continuum flow, particularly, the no-slip boundary condition is assumed to be applicable at the channel wall. However, it has been speculated by a few investigators that slip flow may occur in microchannel flow. Arkilic et al. [17] investigated gaseous

helium flow through microchannels of 1.33 μm in height for pressure drop from 0.2–1.5 atm. It was shown that the Navier–Stokes equations with slip flow boundary condition can give a good estimate of the flow situation. Choi [28] also conducted experiments on gaseous nitrogen flow in circular microtubes with diameters ranging from 2–81 μm. He found that slip flow must be considered for the tube diameter less than 3 μm. On the other hand, for liquid flow, Russian scientists [29] discovered from experiments that the conditions for the slip flow to occur depend on not only the size of channels but also the characteristics of fluid and channel surfaces. It was found that the liquid slip flow may have appreciable effects when non-polar fluid flow over hydrophilic solid surfaces or aqueous solution flow over hydrophobic solid surfaces in microtubes with the diameter less than 2 μm. Although it is still being debated that when slip flow effects become important as channel size decreases, the aqueous solution flow in a hydrophilic silicon channel of tens of microns considered in this work can certainly be treated as a no-slip flow.

By using the Green's function formulation, the solution of equation (13) subjecting to the above boundary conditions can be expressed as

$$\bar{u}(Y,Z) = -\lim_{t\to\infty}\int_{\tau=0}^{t} \mathrm{d}\tau \int_{Y'=0}^{H/D_h}\int_{Z'=0}^{W/D_h} G(Y,Z,t \mid Y',Z',\tau) \times\left[\frac{\mathrm{d}\bar{P}}{\mathrm{d}\bar{X}} + \bar{G}_1\bar{E}_x \sinh\Psi(Y',Z')\right]\mathrm{d}Y'\,\mathrm{d}Z'. \quad (15)$$

Here $G(Y,Z,t \mid Y',Z',\tau)$ is the Green's function which may be found by using the separation of variables method [30]. The expression for $G(Y,Z,t \mid Y',Z',\tau)$ is given by

$$G(Y,Z,t \mid Y',Z',\tau) = \frac{4D_h^2}{WH}\sum_{m=1}^{\infty}\sum_{n=1}^{\infty}\exp\left\{-\pi^2 D_h^2\left[\frac{m^2}{H^2}+\frac{(2n-1)^2}{4W^2}\right](t-\tau)\right\} \times\sin\left(\frac{m\pi D_h}{H}Y\right)\sin\left(\frac{m\pi D_h}{H}Y'\right) \times\cos\left[\frac{(2n-1)\pi D_h}{2W}Z\right]\cos\left[\frac{(2n-1)\pi D_h}{2W}Z'\right]. \quad (16)$$

Substituting equation (16) into equation (15) and rearranging it, one can obtain the non-dimensional fluid velocity profile in the microchannel as follows:

$$\bar{u}(Y,Z) = -\frac{8}{\pi^4 D_h^2}\frac{\mathrm{d}\bar{P}}{\mathrm{d}\bar{X}} \times\sum_{m=1}^{\infty}\sum_{n=1}^{\infty}\frac{(-1)^n[(-1)^m-1]\sin\left(\frac{m\pi D_h}{H}Y\right)\times\cos\left[\frac{(2n-1)\pi D_h}{2W}Z\right]}{m(2n-1)\left[\frac{m^2}{H^2}+\frac{(2n-1)^2}{4W^2}\right]} - \frac{4}{\pi^4 HW}\bar{G}_1\bar{E}_x\sum_{m=1}^{\infty}\sum_{n=1}^{\infty}\frac{\sin\left(\frac{m\pi D_h}{H}Y\right)\cos\left[\frac{(2n-1)\pi D_h}{2W}Z\right]}{\frac{m^2}{H^2}+\frac{(2n-1)^2}{4W^2}} \times\int_{Y'=0}^{H/D_h}\int_{Z'=0}^{W/D_h}\sin\left(\frac{m\pi D_h}{H}Y'\right) \times\cos\left[\frac{(2n-1)\pi D_h}{2W}Z'\right]\sinh\Psi(Y',Z')\,\mathrm{d}Y'\,\mathrm{d}Z'. \quad (17)$$

If there is no electrostatic interaction, the second term on the right hand side of the above equation vanishes. The fluid velocity reduces to

$$\bar{u}_0(Y,Z) = -\frac{8}{\pi^4 D_h^2}\frac{\mathrm{d}\bar{P}}{\mathrm{d}\bar{X}} \times\sum_{m=1}^{\infty}\sum_{n=1}^{\infty}\frac{(-1)^n[(-1)^m-1]\sin\left(\frac{m\pi D_h}{H}Y\right)\times\cos\left[\frac{(2n-1)\pi D_h}{2W}Z\right]}{m(2n-1)\left[\frac{m^2}{H^2}+\frac{(2n-1)^2}{4W^2}\right]} \quad (18)$$

which is the well-known Poiseuille flow velocity profile through the rectangular channel.

Using equations (17) and (18), the mean velocity with and without the consideration of the effects of the EDL may be written, respectively, as

$$\bar{u}_{ave} = -\frac{16HW}{\pi^6 D_h^4}\frac{\mathrm{d}\bar{P}}{\mathrm{d}\bar{X}} \times\sum_{m=1}^{\infty}\sum_{n=1}^{\infty}\frac{[(-1)^m-1]^2}{m^2(2n-1)^2\left[\frac{m^2}{H^2}+\frac{(2n-1)^2}{4W^2}\right]} - \frac{8}{\pi^4 D_h^2}\bar{G}_1\bar{E}_x \times\sum_{m=1}^{\infty}\sum_{n=1}^{\infty}\frac{(-1)^n[(-1)^m-1]}{m(2n-1)\left[\frac{m^2}{H^2}+\frac{(2n-1)^2}{4W^2}\right]} \times\int_{Y'=0}^{H/D_h}\int_{Z'=0}^{W/D_h}\sin\left(\frac{m\pi D_h}{H}Y'\right) \times\cos\left[\frac{(2n-1)\pi D_h}{2W}Z'\right]\sinh\Psi(Y',Z')\,\mathrm{d}Y'\,\mathrm{d}Z' \quad (19)$$

and

$$\bar{u}_{0ave} = -\frac{16HW}{\pi^6 D_h^4}\frac{d\bar{P}}{d\bar{X}} \times \sum_{m=1}^{\infty}\sum_{n=1}^{\infty}\frac{1}{m^2(2n-1)^2\left[\frac{m^2}{H^2}+\frac{(2n-1)^2}{4W^2}\right]}. \quad (20)$$

Thus, the non-dimensional volume flow rate through the rectangular microchannel, defined by $\bar{Q}_v = Q_v/2HWU$, is given by

$$\bar{Q}_v = \bar{u}_{ave}. \quad (21)$$

Correspondingly, in the absence of the electrical double layer, the non-dimensional volume flow rate is expressed as

$$\bar{Q}_{0v} = \bar{u}_{0ave}. \quad (22)$$

In order to calculate the fluid velocity distributions, the analytical solution equation (17) for the velocity is used to obtain the 'exact solution' which, in practice, usually means an error of 0.01% or less. As seen from equation (17), the velocity distribution finally is expressed by two infinite series. Therefore, usually a very large number of terms in series is needed to achieve this error criteria. To reduce computation time, the Aitken's procedure [30] is employed.

4. Electrokinetic potential in a rectangular microchannel

So far, we have derived the distribution of the non-dimensional electrical potential and the net electrical charge density, equation (7) and equation (8), and the non-dimensional fluid velocity profile and mean velocity, equation (17) and equation (19). However, as seen from equations (17) and (19), the local and the mean velocity can be calculated only when the non-dimensional induced electrical potential, $\bar{E}_x$, is known. As explained previously, the pressure-driven liquid flow makes the counterions net charge in the diffuse double layer move to the downstream end. The movement of electrical charges forms an electrical current, called the streaming current, flowing the same direction as the liquid flow. Correspondingly, a flow-induced electric potential, i.e. the electrokinetic potential, is set up along a microchannel. This potential in turns generates an electric current, called the conduction current, to flow in the opposite direction to the pressure-driven liquid flow. When the conduction current I_c is equal to the streaming current I_s, a steady state is reached. Then the net electrical current I should be zero.

$$I = I_s + I_c = 0. \quad (23)$$

The electrokinetic potential at the steady-state is called the streaming potential.

Due to symmetry of the rectangular microchannel, the electrical streaming current I_s is defined as [18]

$$I_s = 2D_h^2 U\int_{Y=0}^{H/D_h}\int_{Z=0}^{W/D_h}\bar{u}(Y,Z)\rho_e(Y,Z)\,dY\,dZ. \quad (24)$$

The electrical conduction current I_c in the microchannel consists of two parts [18]: one is due to the conductance of the bulk liquid; the other is due to the surface conductance or the conductance of the compact layer of the EDL. This electrical conduction current can be expressed as

$$I_c = I_{bc} + I_{sc} = \lambda_t E_x A_c = \frac{2\lambda_t HW\zeta_0}{D_h Re_0}\bar{E}_x \quad (25)$$

where I_{bc} and I_{sc} are the bulk and the surface electrical conduction current, respectively. λ_t is the total electrical conductivity and it can be calculated by $\lambda_t = \lambda_b + (\lambda_s P_s/A_c)$ [18]. Here P_s and A_c are the wetting perimeter and the cross-section area of the channel, respectively, λ_b is the bulk conductivity of the solution, and λ_s is the surface conductivity, which may be determined by experiment [24].

Substituting equation (8) for $\rho_e(Y,Z)$ into equation (24) and putting equations (24) and (25) back into equation (23), one can show that the non-dimensional streaming potential takes the form

$$\bar{E}_x = \frac{D_h^2}{HW}\bar{G}_2\,Re_0\int_{Y=0}^{H/D_h}\int_{Z=0}^{W/D_h}\bar{u}(Y,Z)\sinh\Psi(Y,Z)\,dY\,dZ \quad (26)$$

here the non-dimensional number $\bar{G}_2 = 2zen_0D_hU/\lambda_t\zeta_0$.

Furthermore, the substitution of $\bar{u}(Y,Z)$ from equations (17) and (18) into equation (26) finally gives the non-dimensional streaming potential as

$$\bar{E}_x = \frac{\frac{D_h^2}{HW}\bar{G}_2\,Re_0\int_{Y=0}^{H/D_h}\int_{Z=0}^{W/D_h}\bar{u}_0(Y,Z)\times\sinh\Psi(Y,Z)\,dY\,dZ}{1+\frac{D_h^4}{H^2W^2}\bar{G}_1\bar{G}_2\,Re_0\int_{Y=0}^{H/D_h}\int_{Z=0}^{W/D_h}C_0\times\sinh\Psi(Y,Z)\,dY\,dZ} \quad (27)$$

where

$$C_0 = \frac{4}{\pi^2 D_h^2} \times\sum_{m=1}^{\infty}\sum_{n=1}^{\infty}\frac{\sin\left(\frac{m\pi D_h}{H}Y\right)\cos\left[\frac{(2n-1)\pi D_h}{2W}Z\right]}{\frac{m^2}{H^2}+\frac{(2n-1)^2}{4W^2}} \times\int_{Y'=0}^{H/D_h}\int_{Z'=0}^{W/D_h}\cos\left(\frac{m\pi D_h}{H}Y'\right)\cos\left[\frac{(2n-1)\pi D_h}{2W}Z'\right] \times\sinh\Psi(Y',Z')\,dY'\,dZ'.$$

Once knowing all the parameters shown in equation (27), one can readily determine the non-dimensional streaming potential, which is required to calculate the velocity profile [equation (17)], the mean velocity [equation (19)], and the volumetric flow rate [equation (21)].

5. The electroviscous effect

It is apparent from the previous analysis that the presence of an EDL field and a streaming potential exerts electrical forces on the counterions in the liquid, and hence has a profound influence on the flow behavior. The direct consequence is that a liquid flow is produced in the direction opposite to the pressure-driven flow. Therefore, the flow rate in the pressure drop direction is reduced. The liquid thus appears to exhibit an enhanced viscosity if the flow rate is compared with that in the absence of the EDL.

As we have already shown, the non-dimensional flow rate through the microchannel with and without the consideration of the EDL effects are given by equation (21) and equation (22), respectively. Equalizing equation (21) with equation (22), i.e. $\bar{Q}_{\mathrm{v}} = \bar{Q}_{0\mathrm{v}}$, and using expressions for $\bar{u}_{\mathrm{ave}}$ and $\bar{u}_{0\mathrm{ave}}$ in equation (19) and equation (20) as well as $\mathrm{d}\bar{P}/\mathrm{d}\bar{X}$ and $\bar{E}_{\mathrm{x}}$ in equation (11b), one may get the ratio of the apparent viscosity to the bulk viscosity as

$$\frac{\mu_{\mathrm{af}}}{\mu_{\mathrm{f}}} = \frac{1}{1+\dfrac{\pi^2 D_{\mathrm{h}}^2 \bar{G}_1 \bar{E}_{\mathrm{x}}}{2HW(\mathrm{d}\bar{P}/\mathrm{d}\bar{X})}\dfrac{C_1}{C_2}} \tag{28}$$

where

$$C_1 = \sum_{m=1}^{\infty}\sum_{n=1}^{\infty} \frac{(-1)^n[(-1)^m-1]}{m(2n-1)\left[\dfrac{m^2}{H^2}+\dfrac{(2n-1)^2}{4W^2}\right]} \times \int_{Y'=0}^{H/D_{\mathrm{h}}}\int_{Z'=0}^{W/D_{\mathrm{h}}} \sin\left(\frac{m\pi D_{\mathrm{h}}}{H}Y'\right) \times \cos\left[\frac{(2n-1)\pi D_{\mathrm{h}}}{2W}Z'\right]\sinh\Psi(Y',Z')\,\mathrm{d}Y'\,\mathrm{d}Z'$$

$$C_2 = \sum_{m=1}^{\infty}\sum_{n=1}^{\infty} \frac{[(-1)^m-1]^2}{m^2(2n-1)^2\left[\dfrac{m^2}{H^2}+\dfrac{(2n-1)^2}{4W^2}\right]}.$$

Since the non-dimensional pressure gradient is negative and both C_1 and C_2 are greater than zero, it is easy to show that this ratio is greater than 1, which is referred to as the electroviscous effect [18].

6. Friction coefficient

The friction factor for the flow through rectangular channels in the conventional fluid mechanics is defined as

$$f = \frac{-\dfrac{\mathrm{d}P}{\mathrm{d}x}D_{\mathrm{h}}/4}{\rho_{\mathrm{f}}u_{\mathrm{ave}}^2/2} = \frac{-\dfrac{\mathrm{d}\bar{P}}{\mathrm{d}\bar{X}}}{2\,Re_0\bar{u}_{\mathrm{ave}}^2}. \tag{29}$$

Therefore, the friction coefficient, i.e. the product of the friction factor f and Reynolds number $Re = \rho_{\mathrm{f}}D_{\mathrm{h}}u_{\mathrm{ave}}/\mu_{\mathrm{f}}$, is given by

$$C_{\mathrm{f}} = f\,Re = \frac{-\dfrac{\mathrm{d}\bar{P}}{\mathrm{d}\bar{X}}}{2\bar{u}_{\mathrm{ave}}}. \tag{30}$$

Substituting for $\bar{u}_{\mathrm{ave}}$ in equation (10) leads to

$$C_{\mathrm{f}} = \frac{1}{16}\frac{1}{\dfrac{2HWC_2}{\pi^6 D_{\mathrm{h}}^4}+\dfrac{\bar{G}_1\bar{E}_{\mathrm{x}}C_1}{\pi^4 D_{\mathrm{h}}^2(\mathrm{d}\bar{P}/\mathrm{d}\bar{X})}}. \tag{31}$$

Clearly, if there are no EDL effects, the second term in the denominator of equation (31) will be zero, and hence C_{f} is a constant for a given channel geometry as known in the classical theory of fluid mechanics. However, when the EDL effect is considered, equation (31) shows that C_{f} is no longer a constant, but a function of the EDL field, the streaming potential, and the pressure gradient, etc.

7. Energy equation

In the application of a microchannel heat sink for cooling a microchip, a silicone wafer plate with a large number of microchannels is attached to the chip, as illustrated in Fig. 1(b). The channels are sealed by anodically bonding a glass plate on the top. A liquid is forced to flow through these microchannels to carry the heat away. All microchannels are assumed to have a uniform rectangular cross-section with the same geometric parameters as shown in Fig. 1(a). A microchannel in the center part of the plate will be considered in our analysis below.

As the spatially varying interfacial heat transfer coefficient cannot be prescribed, a conjugate heat transfer problem which consists of simultaneous computation of heat transfer in both the solid channel wall and the cooling liquid has to be solved [31]. However, our objective in this study is to evaluate the influence of electrokinetic effects on convection heat transfer in microchannels. To simplify the problem, an approximation of a uniform heat transfer coefficient along the channel wall is made. This approximation was adopted to perform analysis of heat transfer in microchannels by many other researchers, such as Tuckerman and Pease [2], Keyes [32], Samalam [33], and Bejan and Morega [34]. Under such an approximation, only energy equation for the cooling liquid needs to be considered for the microchannel cooling system.

For a steady-state, fully developed, laminar flow in a

microchannel, the energy equation (with consideration of the axial thermal conduction in flow direction and the viscous dissipation) for the cooling liquid takes the specific form:

$$u\frac{\partial\theta}{\partial x}=\alpha_{\mathrm{f}}\left(\frac{\partial^2\theta}{\partial x^2}+\frac{\partial^2\theta}{\partial y^2}+\frac{\partial^2\theta}{\partial z^2}\right)+\frac{\mu_{\mathrm{f}}}{\rho_{\mathrm{f}}C_{\mathrm{pf}}}\left[\left(\frac{\partial u}{\partial y}\right)^2+\left(\frac{\partial u}{\partial z}\right)^2\right] \tag{32}$$

where θ and α_{f} are the temperature and the thermal diffusivity of the cooling liquid, respectively, C_{pf} is the specific heat capacity of the cooling liquid.

Consider a microchannel in the center part of the plate. Taking advantage of the symmetry of the rectangular channel, we will center the computational domain in a half channel as shown in Fig. 1(a). Thus, the adiabatic condition can be used along the channel symmetric center line, i.e. $(\partial\vartheta/\partial z)=0$ at $z=0$. Uniform heat flux q'' generated by electronic chips is applied to the bottom wall of the channel and may be expressed as $-k_{\mathrm{f}}(\partial\vartheta/\partial y)=q''$ at $y=0$ (here k_{f} is the thermal conductivity of the liquid coolant). Since the thermal conductivity of the glass is about two-order of magnitude lower than that of a silicon wafer, we assume that the top boundary is insulated. This is a conservative assumption which will lead to slight underestimation of the overall heat transfer coefficient. This assumption yields $(\partial\vartheta/\partial y)=0$ at $y=H$. Another approximation made here is that the heat flux along the channel height, q''_y, is uniform, which is identical to the assumption that the heat transfer coefficient along the channel height is constant. For a steady-state heat transfer, an energy balance equation is applied to the wall (silicon wafer) between two channels: $q''d=2q''_yH$ (here d is the thickness of the wall between two channels), which leads to $q''_y=k_{\mathrm{f}}(\partial\vartheta/\partial z)|_{z=W}=(d/2H)q''$. The error induced by this approximation depends upon the ratio of the thermal conductivity of the silicon wafer to that of the cooling liquid and on the geometric ratio of channel height to width as well. As mentioned above, a more precise analysis would require solving a conjugate heat transfer in both solid silicon wafer and cooling liquid simultaneously.

In terms of $\bar{\vartheta}=(\vartheta-\vartheta_i/q''D_{\mathrm{h}}/k_{\mathrm{f}})$, $Pr_{\mathrm{f}}=(\mu_{\mathrm{f}}/\rho_{\mathrm{f}}\alpha_{\mathrm{f}})$, $Ec=(\rho_{\mathrm{f}}U^2/\rho_{\mathrm{f}}C_{\mathrm{pf}}q''D_{\mathrm{h}}/k_{\mathrm{f}})$, $X=(x/D_{\mathrm{h}})$ and the non-dimensional groups in equations (11a) and (11b), the energy equation can be normalized as:

$$\bar{u}\frac{\partial\bar{\vartheta}}{\partial X}=\frac{1}{Re_0\,Pr_{\mathrm{f}}}\left(\frac{\partial^2\bar{\vartheta}}{\partial X^2}+\frac{\partial^2\bar{\vartheta}}{\partial Y^2}+\frac{\partial^2\bar{\vartheta}}{\partial Z^2}\right)+\frac{Ec}{Re_0}\left[\left(\frac{\partial\bar{u}}{\partial Y}\right)^2+\left(\frac{\partial\bar{u}}{\partial Z}\right)^2\right] \tag{33}$$

and the appropriate boundary conditions are:

$$Y=0\quad\frac{\partial\bar{\vartheta}}{\partial Y}=-1\quad Y=\frac{H}{D_{\mathrm{h}}}\quad\frac{\partial\bar{\vartheta}}{\partial Y}=0 \tag{34a}$$

$$Z=0\quad\frac{\partial\bar{\vartheta}}{\partial Z}=0\quad Z=\frac{H}{D_{\mathrm{h}}}\quad\frac{\partial\bar{\vartheta}}{\partial Z}=\frac{d}{2H} \tag{34b}$$

$$X=0\quad\bar{\vartheta}=0. \tag{34c}$$

To consider thermal conduction in axial flow direction, the thermal boundary condition at the outlet of the channel has to be specified. Unfortunately, this information is not usually available. Taking advantage of the numerical scheme, we choose this thermal boundary condition in such a way that the temperature gradient at the outlet of the channel is equal to that of its adjacent upstream grid point. The validity of such a boundary condition at the outlet of the channel will be seen from the calculated results shown later.

Based on the thermal energy balance on the channel length L, the non-dimensional temperature at the outlet of the channel can be expressed as:

$$\bar{\vartheta}_0=\left(\frac{1}{2H}+\frac{d}{4HW}\right)\frac{L}{Re_0\,Pr_{\mathrm{f}}}+\frac{2L}{H+W}\frac{Ec}{Re_0}\int_{Y=0}^{H/D_{\mathrm{h}}}\int_{Z=0}^{H/D_{\mathrm{h}}}\left[\left(\frac{\partial\bar{u}}{\partial Y}\right)^2+\left(\frac{\partial\bar{u}}{\partial Z}\right)^2\right]\mathrm{d}Y\,\mathrm{d}Z. \tag{35}$$

By definition, the non-dimensional bulk mean temperature is calculated at the axial position in the following way:

$$\bar{\vartheta}_{\mathrm{b}}(X)=\frac{D_{\mathrm{h}}^2}{HW\bar{u}_{\mathrm{av}}}\int_{Y=0}^{H/D_{\mathrm{h}}}\int_{Z=0}^{W/D_{\mathrm{h}}}\bar{\vartheta}\bar{u}\,\mathrm{d}Y\,\mathrm{d}Z. \tag{36}$$

Before solving the energy equation, it should be pointed out that the problem we are dealing with is extremely complicated. In principle, the Poisson–Boltzmann equation, the equation of motion, and the energy equation are coupled. On the one hand, the presence of the EDL field and the flow-induced electrokinetic field may cause a deviation of the Poiseuille flow pattern. Consequently, such a 'distorted' (compared with the Poiseuille flow) flow field expressed by equation (17) will have impact on heat transfer in microchannels via the energy equation (32). On the other hand, a change in temperature may affect the EDL field and hence the fluid velocity profile. Such influences are reflected from the non-dimensional electrokinetic diameter $K=\kappa D_{\mathrm{h}}$, or more precisely from the so-called Debye–Huckel parameter defined as $\kappa=(2z^2e^2n_0/\varepsilon_{\mathrm{r}}\varepsilon_0k_{\mathrm{b}}T)^{1/2}$. Fortunately, our calculations showed that the effects of temperature on the EDL field and the fluid velocity field are negligible. This can be understood as follows: it should be noted that the dielectric constant is dependent on temperature. For aqueous solutions the dielectric constant monotonically changes in an opposite way to temperature variation [35]. This means if temperature increases, the dielectric constant will decrease. Thus, the dependence of

Debye–Huckel parameter on temperature is very weak. Consider the following simple example. For a single phase convection, the inlet and the outlet temperature are chosen as $T_1 = 298$ K (25°C) and $T_2 = 335$ K (80°C), respectively. The corresponding dielectric constant are 78.5 and 61.0, respectively [35]. A simple calculation shows that the ratio of the Debye–Huckel parameter is $(\kappa_2/\kappa_1) = 1.04$. Accordingly, the ratio of the calculated mean velocity in such an extreme case is $(\bar{u}_{ave2}/\bar{u}_{ave1}) = 1.01$ only. Therefore, we can safely assume that the Poisson–Boltzmann equation is decoupled from the energy equation in our calculations.

The energy equation is computed by using the control-volume based finite difference method [27]. Since the flow and the heat transfer are decoupled and the velocity field has already been solved before, the viscous dissipation term can be easily treated as the source term, which is independent of temperature. The upwind scheme is employed to approximate the convection term. Central differences are used to discrete the diffusion terms. To validate the numerical code, the program was tested by reproducing the same heat transfer problem as stated by Chandrupatla and Sastri [36]. The grid-dependence of the results was verified by repeating the same calculation for various numbers of grid points.

After the temperature distribution is obtained, the local Nusselt number at each axial step can be computed by

$$Nu_{X,H_2} = \frac{h_x D_h}{k_f} = \frac{d+2W}{2(H+2W)} \frac{1}{\vartheta_s(X) - \vartheta_b(X)} \tag{37}$$

where h_x is the local heat-transfer coefficient and ϑ_s is the non-dimensional average temperature of the channel wall. The mean Nusselt number is given by:

$$Nu_{ave,H_2} = \frac{D_h}{L} \int_{Z=0}^{L/D_h} Nu_{X,H_2} \, dX. \tag{38}$$

8. Results and discussion

In the previous sections, general equations were derived for characterizing the pressure-driven liquid flow and heat transfer through a rectangular microchannel. Examination of these equations reveals that the characteristics of such forced microchannel flow and heat transfer are determined by following non-dimensional parameters K, $d\bar{P}/d\bar{X}$, $\bar{G}_1$, $\bar{G}_2$, and Ec. Physically, the non-dimensional electrokinetic diameter, $K = \kappa D_h$, represents the ratio of the hydraulic diameter of a rectangular channel to the thickness of the EDL. By definition, the non-dimensional pressure gradient, $d\bar{P}/d\bar{X} = [D_h(dP/dx)/\mu_f U]$, can be interpreted as the ratio of the mechanical force to the viscous force. $\bar{G}_1 = (2zen_0\zeta_0/\rho_f U^2)$ characterizes the ratio of the EDL energy to the mechanical kinetic energy. $\bar{G}_2 = (2zen_0 D_h U/\lambda_t \zeta_0)$ represents the ratio of the streaming current to the conduction current. Eckert number, Ec, measures the viscous dissipation effect.

In order to estimate the values of these non-dimensional parameters, we consider a fully developed, laminar flow of an aqueous 1:1 electrolyte (e.g., KCl) solution through a rectangular microchannel with a height of 20 μm, width of 30 μm and length of 1 cm. At a typical room temperature $T = 298$ (K), the dielectric constant and the viscosity of the liquid are $\varepsilon_r = 78.5$ and $\mu_f = 0.90 \times 10^{-3}$ (kg ms^{-1}), respectively. An applied pressure difference of $\Delta P = 2$ (atm) and an arbitrarily chosen reference velocity $U = 1.0$ (m s^{-1}) are considered. An experimentally determined correlation [24] for the zeta potential of the P-type silicon plates with different concentrations of KCl electrolyte solution is used in our calculation. For electronic cooling systems, the fluid temperature at the entrance of the channel and the heat flux are chosen as 298 K and 1.0×10^5 W m^{-2}, respectively.

With the above mentioned values, it is quite straightforward to calculate the flow and heat transfer characterizing parameters, such as velocity distribution, flow rate, friction constant, temperature distribution, and Nusselt number by the equations developed above.

8.1. EDL potential profile

The non-linear, two-dimensional Poisson–Boltzmann equation is computed for two sets of concentrations and zeta potentials: $c_{01} = 10^{-6}$ M ($n_{01} = 6.022 \times 10^{20}$), $\zeta_{c1} = 150$ mV and $c_{02} = 10^{-8}$ M ($n_{02} = 6.022 \times 10^{18}$), $\zeta_{c2} = 200$ mV. The results for the non-dimensional EDL potential profile across a quarter of the rectangular channel are plotted in Fig. 2(a)–(b). As seen in Fig. 2, the EDL field exists only in the region close to the channel wall for the concentration $c_{01} = 10^{-6}$ M in Fig. 2(a). However, the electrical potential profile can extend to a much larger portion of the channel for the concentration $c_{02} = 10^{-8}$ M in Fig. 2(b). This indicates that the EDL effects may be significant for lower concentration aqueous solutions. Closer examination of Fig. 2 reveals the strong corner effect on the EDL potential profile. This is an important feature of the two-dimensional Poisson–Boltzmann equation which is expected to influence the flow field in such a rectangular microchannel.

8.2. Velocity distribution

The computation of non-dimensional velocity distribution according to equation (17), which is an exact solution to the equation of motion by the Green's function formula, is carried out for a given external pressure difference. In Fig. 3(a)–(d), the distribution of non-dimensional velocity is plotted for two different microchannels of 30×20 μm and 30×40 μm with and without the consideration of the EDL effects. As seen from these

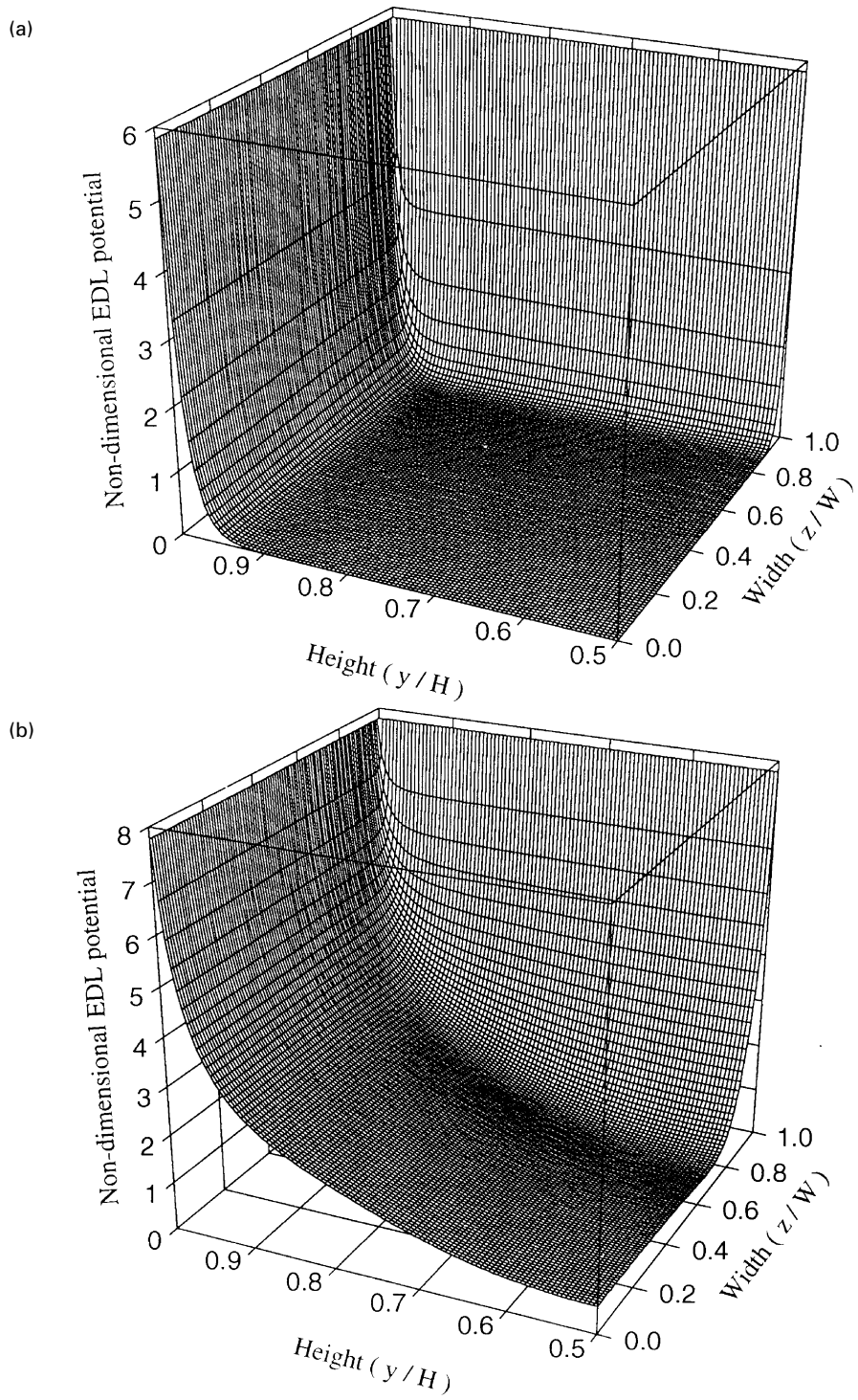

Fig. 2. Non-dimensional EDL potential profile (in one quarter of cross-sectional microchannel with width 30 μm and height 20 μm). (a) $c_{01} = 10^{-6}$ M, $\zeta_{c1} = 150$ mV. (b) $c_{02} = 10^{-8}$ M, $\zeta_{c2} = 200$ mV.

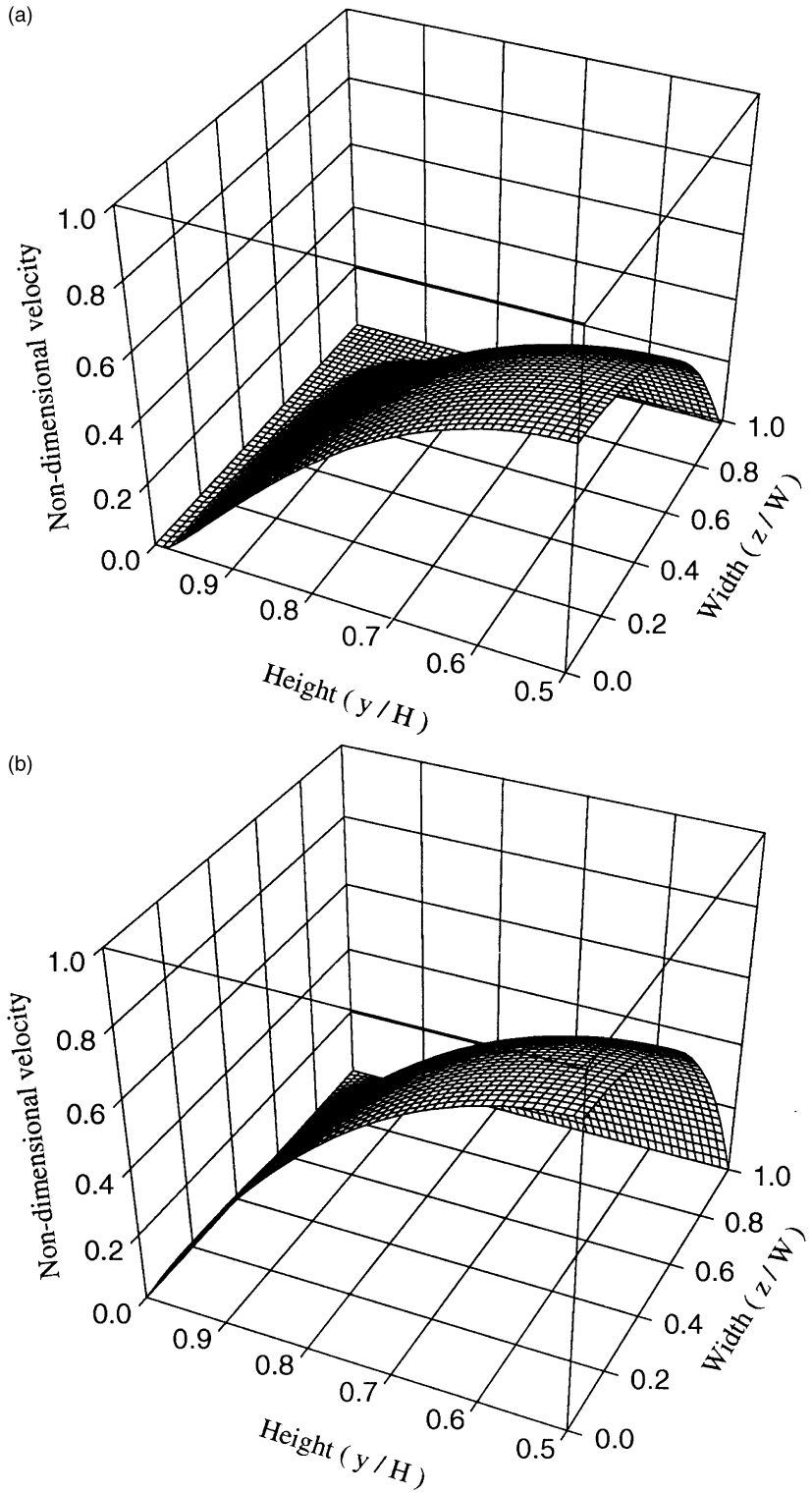

Fig. 3. Non-dimensional velocity distribution (in one quarter of cross-sectional microchannel). (a)(c) With EDL effects ($c_0 = 10^{-8}$ M, $\zeta_c = 200$ mV) for channel 30×20 and 30×40 μm, respectively. (b)(d) Poiseuille profile for channel 30×20 and 30×40 μm, respectively.

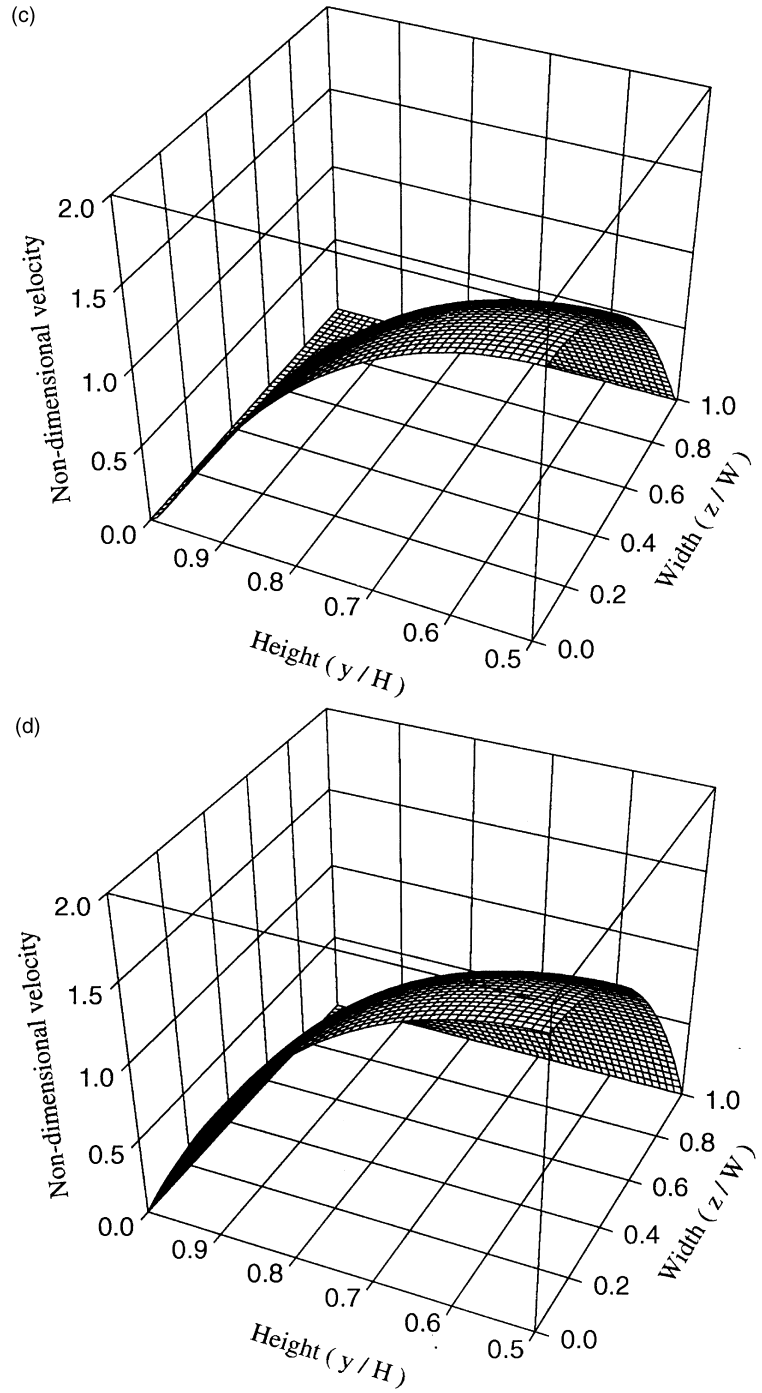

Fig. 3—*continued.*

figures, the EDL exhibits significantly stronger effects on the flow pattern in the smaller channel in Fig. 3(a) than that in the larger channel in Fig. 3(c). In Fig. 3(a) and (c), it is clearly shown that the velocity distributions are distorted and the flow velocity near the channel wall approaches zero due to the action of the EDL field and the induced electrokinetic potential. Also the maximum velocity at the center of the channel are much lower than that in the classical Poiseuille flow in Fig. 3(b) and (d). Moreover, as expected from the two-dimensional P–B

equation, the flow fields around the channel corner in Fig. 3(a) and (c) deviate from the classical Poiseuille flow pattern in Fig. 3(a) and (c), respectively.

8.3. Volumetric flow rate

As explained before, the streaming potential drives counterions in the diffuse double layer to move in the opposite direction to the pressure-driven flow and these moving ions drag the surrounding liquid molecules with them. This produces a reduced volumetric flow rate as predicted by equation (21). The result is demonstrated in Fig. 4, which depicts the volumetric flow rate as a function of the non-dimensional pressure difference for two sets of concentrations and zeta potentials. Obviously Fig. 4 shows for a lower concentration of the electrolyte solution and a higher zeta potential of the channel wall, the volumetric flow rate is remarkably reduced. The explanation for this is that if the ionic concentration is lower, which implies a smaller Debye–Huckel parameter, i.e. a larger EDL thickness, the EDL exhibits stronger effects.

8.4. Friction coefficient

In Fig. 5, the friction coefficient C_f, which is the product of the friction factor and Reynolds number as given by equation (31), is plotted against the microchannel height with a fixed channel width for two sets of concentrations and zeta potentials. It is well known that from the classical theory (no EDL effects) the friction coefficient for a rectangular channel is only dependent on the geometric ratio of channel height to width. However, the calculations from our model indicate that the zeta potentials of the solid surface and the concentrations of the electrolyte solution have a significant influence on the friction coefficient. For the case of a smaller value of the zeta potential and a higher ionic concentration, the friction coefficient is very close to that predicted by the classical theory. But as the zeta potential increases and the ionic concentration decreases, which implies stronger electroviscous effects, the friction coefficient drastically increases. The presented result of the friction coefficient dependence of the ratio of channel height to width is in a rough agreement with that obtained by Peng–Peterson–Wang's papers [10, 12].

8.5. Temperature field and Nusselt number

Generally, the effects of EDL and electrokinetic fields reduce the liquid velocity and the flow rate, and consequently increase the temperature in the microchannel.

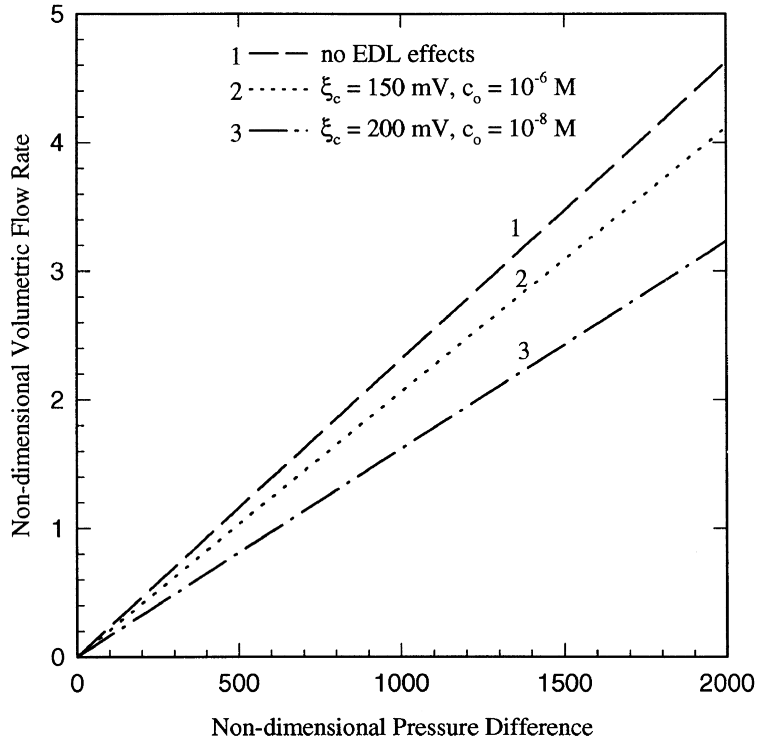

Fig. 4. Variation of non-dimensional volumetric flow rate with non-dimensional pressure difference for different concentrations and zeta potentials.

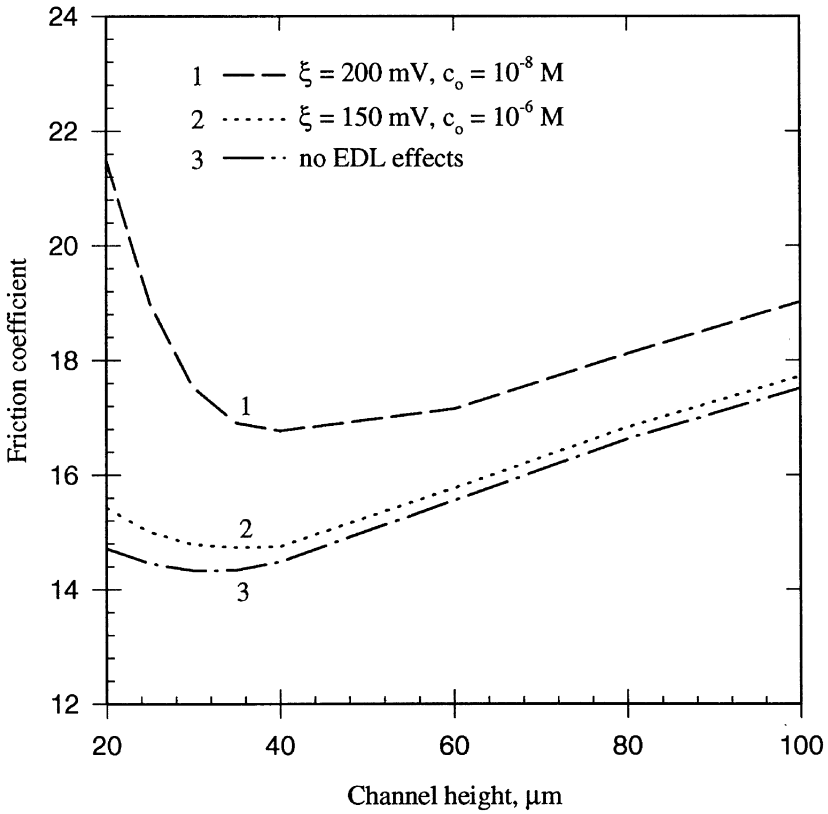

Fig. 5. Friction coefficient vs microchannel height with a fixed width of 30 μm for different concentrations and zeta potentials.

Such effects on the temperature field are clearly shown in Fig. 6(a)–(d), which depict the non-dimensional cross-sectional temperature distribution at the middle cross-section of the microchannel for two different channels 30×20 and 30×40 μm, respectively. The general trend is that the smaller channel suffers much stronger EDL effects than the larger one. This may be understood as follows: as the channel size gets smaller, the EDL thickness becomes relatively larger and hence its effects become stronger. In Fig. 7, the local non-dimensional bulk mean temperature of the fluid is plotted as a function of the channel length. Basically it shows a good linear relation of temperature variation with the channel length. This result verifies the validity of the temperature boundary condition we specified at the exit of the microchannel. From both Figs 6 and 7, a conclusion may be drawn: under the conditions in our calculations, the EDL effects on microchannel flow and heat transfer may become unimportant when the channel size is larger than 40 μm. This accords with the fact reported by Pfahler et al. [6, 7] that deviations from the classical Poiseuille flow were experimentally observed in the small channels (hydraulic diameter less than 40 μm).

To see the overall heat transfer characteristics, the local Nusselt number vs the channel length with/without consideration of the EDL effects for the channel of 30×20 μm is shown in Fig. 8. It is seen that the Nusselt number with the consideration of the EDL effects is lower than that in conventional theory. For the limiting Nusselt numbers the difference is over 10%. Moreover, it is observed that for a fully developed, hydrodynamic flow the thermal entrance effect on the microchannel heat transfer can be neglected as it occupies only 1–2% of the channel length. Figure 9 depicts the mean Nusselt number as a function of the microchannel height with a fixed width of 30 μm. Again there is quite a difference between the mean Nusselt numbers with and without the consideration of the EDL effects. Also, closer examination of Fig. 9 indicates that this difference becomes smaller as the channel height increases and tends to be a constant when the channel height is larger than 40–50 μm. The reason is that when the channel height becomes larger the EDL effects become smaller. When the channel height is over 40–50 μm, the EDL effects are not from the channel height but from the channel width, which is fixed at 30 μm.

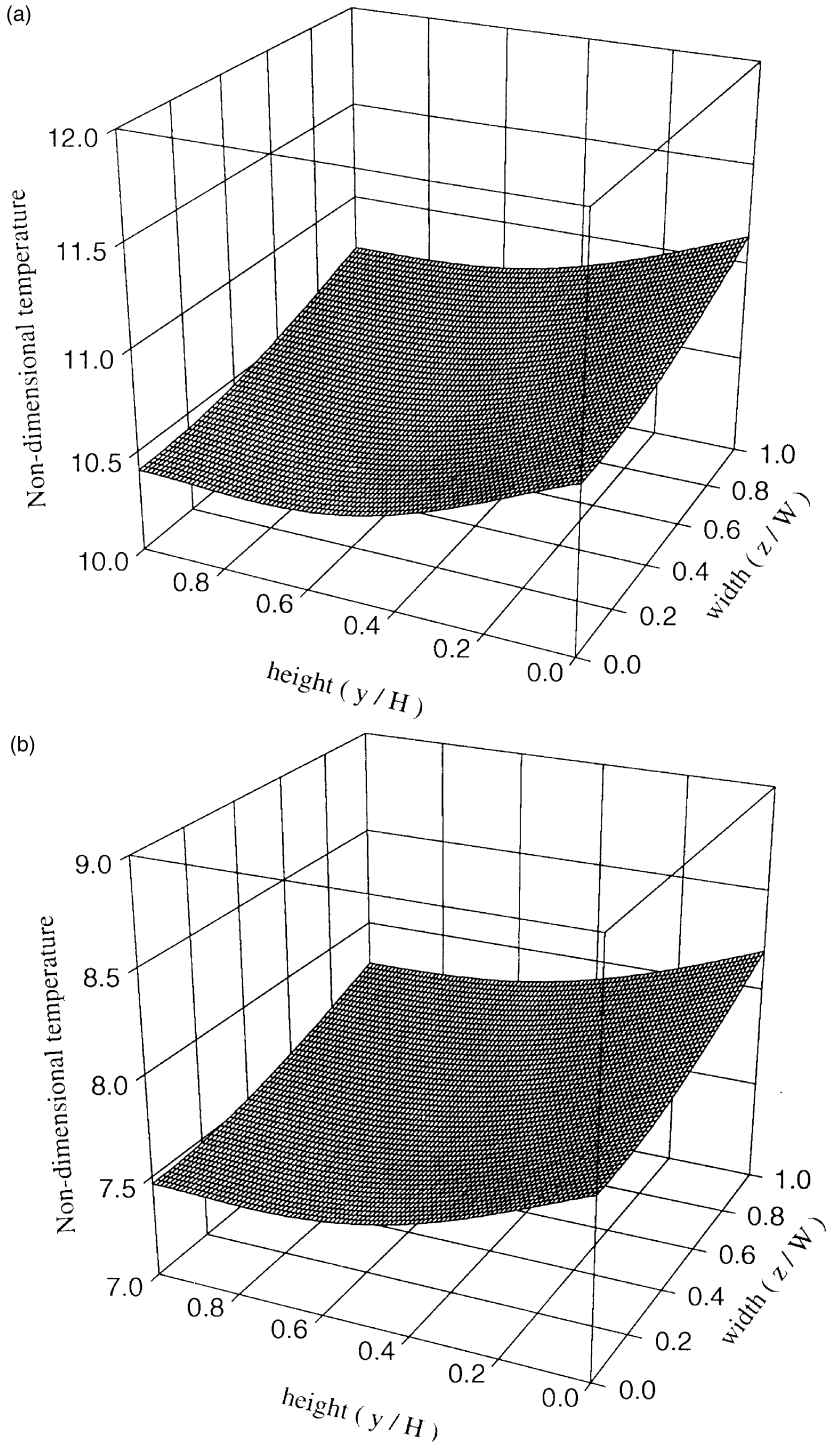

Fig. 6. Non-dimensional temperature distribution (in a half channel at the middle cross-section of a microchannel). (a)(c) With EDL effects ($c_0 = 10^{-8}$ M, $\zeta_e = 200$ mV) for channel 30×20 and 30×40 μm, respectively. (b)(d) No EDL effects for channel 30×20 and 30×40 μm, respectively.

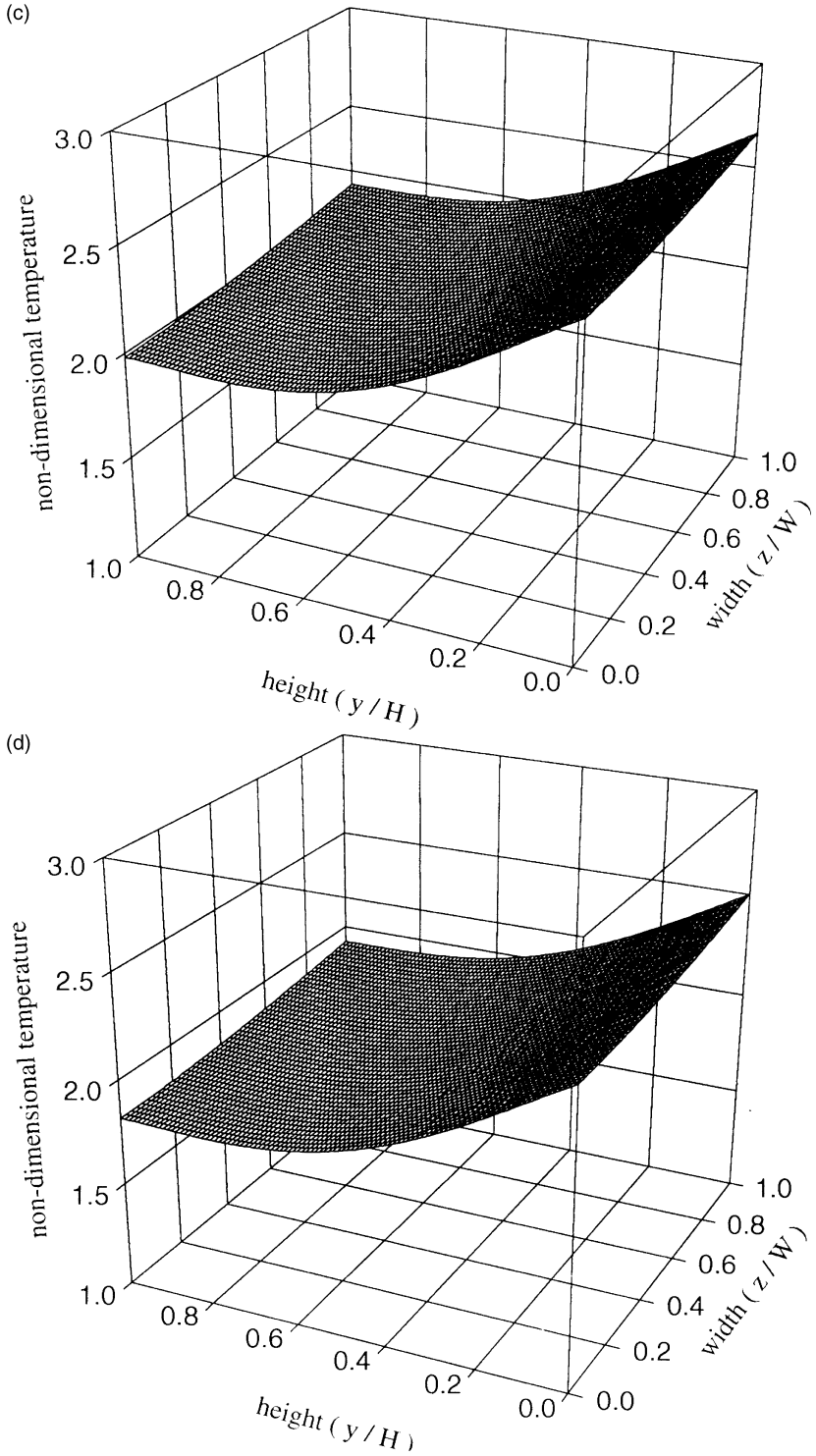

Fig. 6—*continued.*

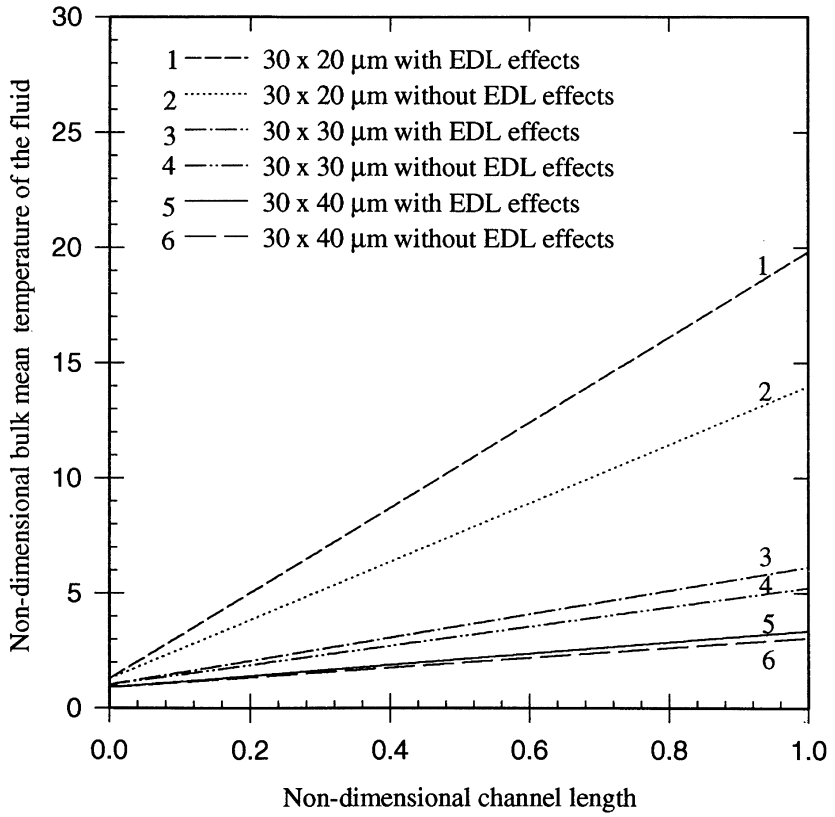

Fig. 7. Local non-dimensional bulk mean temperature of the liquid vs non-dimensional channel length for different channel sizes (with EDL effects: $c_0 = 10^{-8}$ M, $\zeta_c = 200$ mV).

In addition, numerical tests were performed to evaluate the influences of the axial thermal conduction in flow direction and the viscous dissipation considered in the energy equation (33). These effects are usually ignored in macrochannel heat transfer treatment. It was found that for the parameters chosen in this study the consideration of the axial thermal conduction in flow direction only causes a 0.03% increase in the non-dimensional bulk mean temperature at the outlet of the channel and a 0.02% change of the mean Nusselt number, respectively. Similarly, the consideration of the viscous dissipation only causes a 0.05% increase in the non-dimensional bulk mean temperature at the outlet of the channel and a 0.6% change of the mean Nusselt number, respectively. These results clearly show that the axial thermal conduction in flow direction and the viscous dissipation have little impact on microchannel heat transfer and therefore they can be safely neglected. As such, it can be concluded that the existence of anomalous behavior of heat transfer in microchannels should be attributed to the effects that influence the flow characteristics, such as the electrokinetic effects.

9. Concluding remarks

The effects of the EDL at the solid–liquid interface on the pressure driven liquid flow and heat transfer through a rectangular microchannel are analyzed in this work. The computational results show the EDL potential profile exhibits different features from that predicted by the one-dimensional P–B equation and shows strong corner effects. The EDL field near the channel wall tends to restrict the motion of ions and hence the liquid molecules in the EDL region. For the cases of low concentration solutions and high zeta potentials, the velocity distribution, the volumetric flow rate, and the temperature field are significantly affected by the presence of the EDL and hence deviate from the prediction of the conventional theory. The EDL field and the induced electrokinetic potential act against the liquid flow, resulting in a higher friction coefficient, a reduced flow rate, and a reduced Nusselt number, depending on the geometric parameters of the rectangular microchannels, the ionic concentration of solutions, and the zeta potential of the channel wall. Some experimentally observed anomalous phenomena

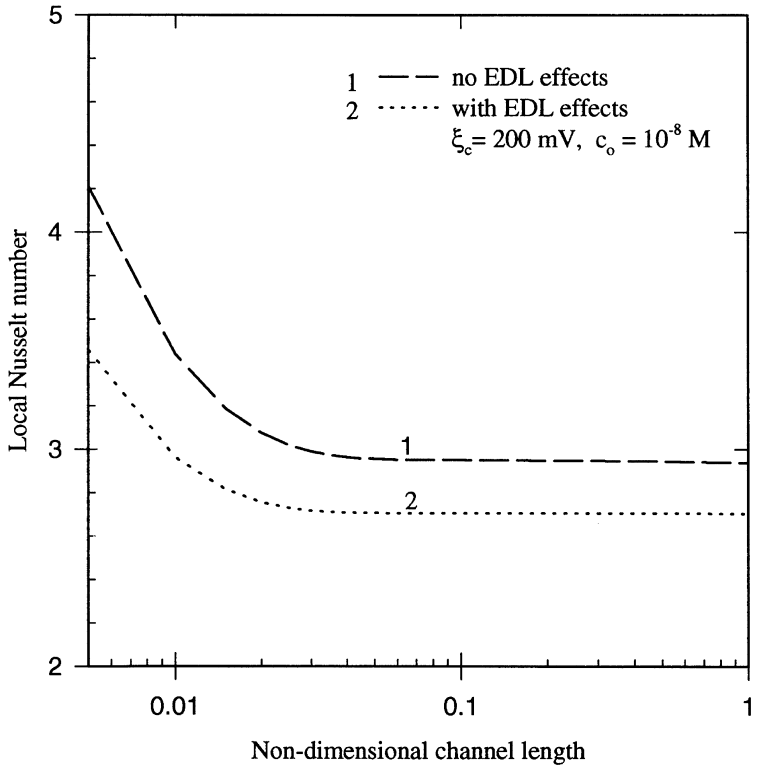

Fig. 8. Local Nusselt number vs non-dimensional microchannel length.

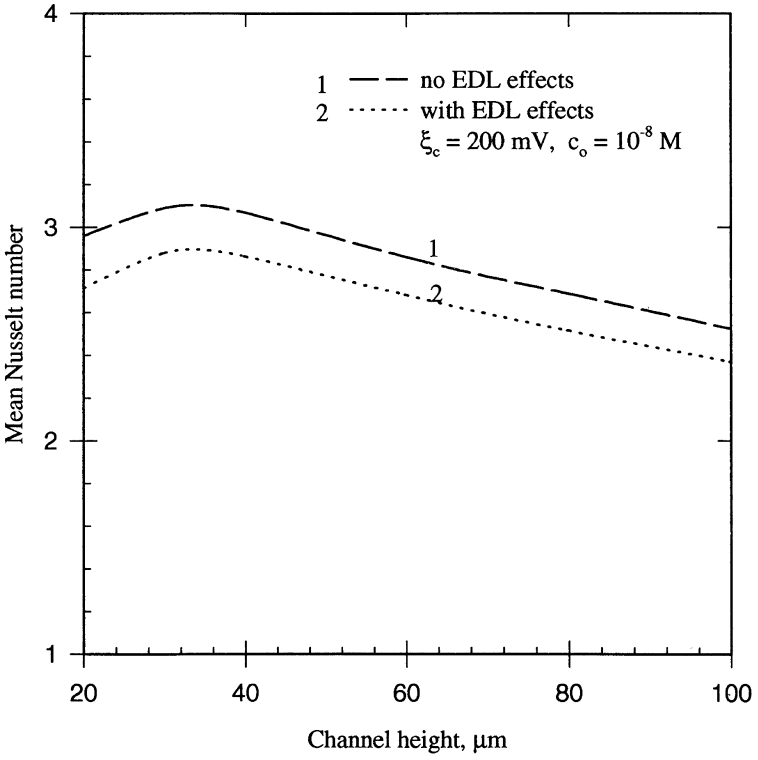

Fig. 9. Mean Nusselt number vs microchannel height with a fixed width of 30 μm.

may be explained using the models developed in this work.

Appendix

In the following, we will discuss the validity of the Boltzmann distribution in the case of the microchannel flow.

Generally, the ionic concentration distribution n_i is described by the Nernst–Planck equation [26], which under steady-state conditions and in the absence of source terms can be expressed in the convective-diffusion form

$$\nabla\cdot(D_i\nabla n_i)-\nabla\cdot(\mathbf{V}_i\cdot n_i)=0 \tag{A1}$$

where D_i is the diffusion coefficient of the type-i ion and $\mathbf{V}_i$ is the velocity of the type-i ion. Under such a situation, the ion velocity $\mathbf{V}_i$ can be decomposed into contributions from hydrodynamic velocity $\mathbf{V}$ and a velocity $\mathbf{u}_i$ due to the electrostatic field acting on the ion (caused by the presence of the EDL field). Then one can write

$$\mathbf{V}_i=\mathbf{V}+\mathbf{u}_i. \tag{A2}$$

The velocity $\mathbf{u}_i$ is related to the electrostatic force exerting on the ions by the following equation

$$\mathbf{F}_{ei}=z_ie\mathbf{E}=f_i\mathbf{u}_i \tag{A3}$$

where z_i is the valence of the type-i ion, e is the elementary charge, $\mathbf{E}$ is the electrostatic field strength, and f_i is the hydrodynamic resistance coefficient. Noting that $\mathbf{E}$ is given by

$$\mathbf{E}=-\nabla\psi \tag{A4}$$

(here ψ is the electrical potential) and the hydrodynamic resistance coefficient f_i can be determined from the Stokes–Einstein equation

$$f_i=\frac{k_bT}{D_i} \tag{A5}$$

(here k_b is the Boltzmann constant), one can readily show that the velocity $\mathbf{u}_i$ can be given by

$$\mathbf{u}_i=-\frac{z_ieD_i\nabla\psi}{k_bT}. \tag{A6}$$

Substituting equations (A6) and (A2) into equation (1), and using $\nabla\cdot\mathbf{V}=0$, yields

$$\nabla^2n_i-\frac{\mathbf{V}}{D_i}\cdot\nabla n_i+\nabla\cdot\left(\frac{z_ien_i}{k_bT}\nabla\psi\right)=0. \tag{A7}$$

The equation (A7) can be normalized as

$$\nabla^2\bar{n}_i-Pe\,\mathbf{e}_\mathbf{V}\cdot\nabla\bar{n}_i+\nabla\cdot\left(\frac{z_ie\bar{n}_i}{k_bT}\nabla\psi\right)=0 \tag{A8}$$

where $\bar{n}_i$ is the non-dimensional ionic concentration $\bar{n}_i=(n_i/n_{i0})$ (here n_{i0} is the bulk concentration of the type-i ion), Pe is the Peclet number $Pe=(|\mathbf{V}|D_h/D_i)$, $\mathbf{e}_\mathbf{V}$ is the unit vector along the hydrodynamic velocity $\mathbf{V}$ direction.

(i) Considering a micromchanel flow with a very small Peclet number, i.e. $Pe\approx0$, the second term in the equation (A8) drops out and then equation (A8) becomes

$$\nabla^2\bar{n}_i+\nabla\cdot\left(\frac{z_ie\bar{n}_i}{k_bT}\nabla\psi\right)=0. \tag{A9}$$

(ii) If the microchannel flow is fully-developed, the components of hydrodynamic velocity $\mathbf{V}$ satisfy $u=u(y,z)$ and $v=w=0$ in terms of Cartesian coordinates. Under such conditions, equation (A8) is reduced to

$$\nabla^2\bar{n}_i-Pe_X\frac{\partial\bar{n}_i}{\partial X}+\nabla\cdot\left(\frac{z_ie\bar{n}_i}{k_bT}\nabla\psi\right)=0. \tag{A10}$$

Note that under steady-state situations no mass exchange occurs at the channel wall. This implies that there is no appreciable ionic concentration gradient along the axial direction, i.e. $(\partial\bar{n}_i/\partial X)=0$. Accordingly, the equation (A10) is also reduced to equation (A9).

In either case (i) or case (ii), one can readily solve equation (A9) and obtain its solution, which is

$$\bar{n}_i=\exp\left(-\frac{z_ie\psi}{k_bT}\right)\quad\text{or } n_i=n_{i0}\exp\left(-\frac{z_ie\psi}{k_bT}\right). \tag{A11}$$

This is the well-known Boltzmann distribution. Therefore, we may conclude that for a microchannel flow with a very small Peclet number or in a fully-developed hydrodynamic state, the Boltzmann distribution equation is still valid.

Acknowledgements

The authors would like to gratefully acknowledge the financial support of the Natural Sciences and Engineering Research Council of Canada. The authors also are grateful to anonymous reviewers for their valuable suggestions.

References

[1] J.M. Cuta, C.E. Bennet, C.E. McDonald, T.S. Ravigururajan, Fabrication and testing of microchannel heat exchangers, Proceedings of Society of Photo-Optical Instrumentation Engineers, Vol. 2640, Washington, DC, 1995, pp. 152–160.

[2] D.B. Tuckerman, R.F.W. Pease, High performance heat sinks for VLSI, IEEE Electron Device Letters 2 (1981) 126–129.

[3] W.J. Bennett, B.L. Freitas, D. Ciarlo, R. Beach, S. Sutton, M. Emanuel, R. Solarz, Microchannel cooled heat sinks for high average power laser diode arrays, Proceedings of Society of Photo-Optical Instrumentation Engineers, Vol. 1997, Washington, DC, 1993, pp. 98–107.

[4] A.B. Duncan, G.P. Peterson, Review of microscale heat transfer, Applied Mechanics Review 47 (1994) 397–428.
[5] J. Goodling, Microchannel heat exchangers—a review, Proceedings of the Society of Photo-Optical Instrumentation Engineers, Vol. 1997, Washington, DC, 1993, pp. 66–82.
[6] J. Pfahler, J. Harley, H. Bau, J. Zemel, Liquid and gas transport in small channels, Microstructure, Sensors and Actuators, ASME, New York, NY, 1990, DSC-Vol. 19, pp. 149–157.
[7] J. Pfahler, J. Harley, H. Bau, J. Zemel, Gas and liquid flow in small channels, Micromechanical Sensors, Actuators and Systems, ASME, New York, NY, 1991, DSC-Vol. 32, pp. 49–60.
[8] W. Urbanek, J.N. Zemel, H.H. Bau, An investigation of the temperature dependence of Poiseuille numbers in microchannel flow, Journal of Micromechanics and Microengineering 3 (1993) 206–209.
[9] M.M. Rahman, F. Gui, Experimental measurements of fluid flow and heat transfer in microchannel cooling passages in a chip substrate, Advances in Electronic Packaging, ASME, 1993, EEP-Vol. 4–2, pp. 685–692.
[10] X.F. Peng, G.P. Peterson, B.X. Wang, Heat transfer characteristics of water flowing through microchannels, Experimental Heat Transfer 7 (1994) 265–283.
[11] X.F. Peng, G.P. Peterson, Forced convection heat transfer of single-phase binary mixtures through microchannels, Experimental Thermal and Fluid Science 12 (1996) 98–104.
[12] B.X. Wang, X.F. Peng, Experimental investigation on liquid forced convection heat transfer through microchannels, International Journal of Heat and Mass Transfer 37 (Suppl. 1) (1994) 73–82.
[13] A.C. Eringen, Simple microfluids, International Journal of Engineering Science 2 (1964) 205–217.
[14] A.C. Eringen, Theory of thermomicrofluids, Journal of Mathematical Analysis and Applications 38 (1972) 480–496.
[15] A.M. Jacobi, Flow and heat transfer in microchannels using a microcontinuum approach, Journal of Heat Transfer 111 (1989) 1083–1085.
[16] A. Beskok, G.E. Karniadakis, Simulation of heat and momentum transfer in complex microgeometries, Journal of Thermophysics and Heat Transfer 8 (1994) 648–655.
[17] E.B. Arkilic, K.S. Breuer, M.A. Schmidt, Gaseous flow in microchannels, Application of Microfabrication to Fluid Mechanics, ASME, 1994, FED-Vol. 197, pp. 57–66.
[18] R.J. Hunter, Zeta Potential in Colloid Science: Principles and Applications, Academic Press, New York, 1981.
[19] S.S. Dukhin, Equilibrium double layer and electrokinetic phenomena, in: E. Matijevic (Ed.), Surface and Colloid Science, Vol. 7, John Wiley and Sons, New York, 1974.
[20] D. Burgreen, F.R. Nakache, Electrokinetic flow in ultrafine capillary slits, Journal of Physical Chemistry, 68 (1964) 1084–1091.
[21] C.L. Rice, R. Whitehead, Electrokinetic flow in narrow cylindrical capillaries, Journal of Physical Chemistry 69 (1965) 4017–4023.
[22] S. Levine, J.R. Marriott, G. Neale, N. Epstein, Theory of electrokinetic flow in fine cylindrical capillaries at high zeta potential, Journal of Colloid and Interface Science 52 (1975) 136–149.
[23] G.M. Mala, D. Li, J.D. Dale, Heat transfer and fluid flow in microchannels, International Journal of Heat and Mass Transfer 40 (1997) 3079–3088.
[24] G.M. Mala, D. Li, C. Werner, H.J. Jacobasch, Y.B. Ning, Flow characteristics of water through a microchannel between two parallel plates with electrokinetic effects, International Journal of Heat and Fluid Flow 18 (1997) 489–496.
[25] T.L. Hoopman, Microchanneled structures, Microstructure, Sensors and Actuators, ASME, New York, NY, 1990, DSC-Vol. 19, pp. 171–174.
[26] T.G.M. van de Ven, Colloidal Hydrodynamics, Academic Press, San Diego, 1989.
[27] S.V. Patankar, Numerical Heat Transfer and Fluid Flow, McGraw-Hill, New York, 1980.
[28] S.B. Choi, Friction factors and heat transfer in microtubes, D.E. dissertation, Louisiana Technical University, LA, 1991.
[29] N.V. Churaev, V.D. Sobolev, A.N. Somov, Slippage of liquids over lyophobic solid surfaces, Journal of Colloid and Interface Science 97 (1984) 547–581.
[30] J.V. Beck, Heat Conduction using Green's Function, Hemisphere, London.
[31] A. Weisberg, H.H. Bau, J.N. Zemel, Analysis of microchannels for integrated cooling, International Journal of Heat and Mass Transfer 35 (1992) 2465–2474.
[32] R.W. Keyes, Heat transfer in forced convection through fins, IEEE Transactions on Electron Devices 31 (1984) 1218–1221.
[33] V.K. Samalam, Convective heat transfer in microchannels, Journal of Electronic Materials 18 (1989) 611–617.
[34] A. Bejan, A.M. Morega, Optimal arrays of pin fins and plate fins in laminar forced convection, Journal of Heat Transfer 115 (1993) 75–81.
[35] R. Weast, M.J. Astle, W.H. Beyer, CRC Handbook of Chemistry and Physics, CRC Press, Inc., Boca Raton, 1986.
[36] A. Chandrupatla, V.M.K. Sastri, Laminar forced convection heat transfer of a non-Newtonian fluid in a square duct, International Journal of Heat and Mass Transfer 20 (1977) 1315–1324.